Trans. JSASS Aerospace Tech. Japan
Vol. 14, No. ists30, pp. Pb_7-Pb_12, 2016

Spatial Profile of Ion Velocity Distribution Function in Helicon High-Density Plasma by Laser Induced Fluorescence Method

By Yuriko TANIDA,[1)] Daisuke KUWAHARA[2)] and Shunjiro SHINOHARA[2)]

[1)] *Institute of Mechanical Systems Engineering, Tokyo University of Agriculture and Technology, Tokyo, Japan*
[2)] *Department of Mechanical Systems Engineering, Tokyo University of Agriculture and Technology, Tokyo, Japan*

(Received July 30th, 2015)

Helicon plasma sources have been studied in many fields across science and technology because they can supply high-density plasmas with a broad range of external operating parameters. In our laboratory, we aim to develop a completely electrodeless electric thruster, which is expected to have a high efficiency and a long lifetime, leading to be useful on a deep space exploration. In order to demonstrate and optimize this thruster system, it is important to have detailed distributions of plasma flow. Laser induced fluorescence (LIF) diagnostics, which can measure velocity distribution functions of particles, has advantages from a view point of, e.g., high resolution in time and space, and it can determine an absolute particle velocity and its temperature in addition to its relative density. Here, we have been developing a LIF measurement system using a Multi-Pixel Photon Counter (MPPC) for a multi-channel system. Argon ion velocity depending on the magnetic field gradient in a downstream region is measured by this LIF system.

Key Words: Electrodeless/Helicon Plasma Thrusters, Diagnostics

Nomenclature

c	:	speed of light
B_z	:	axial magnetic field strength
B_r	:	external radial magnetic field strength
$f(r,v)$	:	ion particle distribution function
F_i	:	thrust by ion
FR	:	flow rate
k	:	Boltzmann constant
N	:	number of electrode magnets
n_e	:	electron density
n_i	:	ion density
m_i	:	ion mass
P_{RF}	:	input power of radio frequency
T_i	:	ion temperature
v	:	particle velocity
μ	:	magnetic moment
ν	:	resonant frequency
$\Delta\nu$	:	frequency shift by Doppler effect
$\Delta\nu_{FWHM}$	:	full width at half maximum of ion velocity distribution function

1. Introduction

Helicon sources[1)] can produce high-density ($\sim 10^{13}$ cm^{-3}) plasmas efficiently with a broad range of external operating parameters such as the fill pressure, the magnetic field strength and its field configuration as long as the excitation frequency is between the ion and electron cyclotron frequencies. Therefore, several kinds of helicon propulsion systems have been studied e.g. Variable Specific Impulse Magnetoplasma Rocket (VASIMR),[2,3)] Helicon Double Layer Thruster (HDLT)[4-6)] and Mini-helicon Plasma Thruster,[7)] including ours.[8)] Electric propulsions are effective for a deep space exploration because of their high specific impulse. The Japanese space probe "Hayabusa",[9)] which had cathode-less electron cyclotron resonance ion engines (but with ion grids directly contacting with plasmas) fulfilled its mission successfully. For the deeper space explorer, high power and high efficiency propulsion system is needed. However, conventional electric propulsion systems sometimes suffer from the problem of finite lifetime caused by the electric erosion, which especially occurs under the high-power operation. In order not to contact the plasma with the electrodes, the completely electrodeless acceleration scheme is effective. Our group has been developing a new electrodeless electric propulsion system with a high efficiency and a long lifetime under the Helicon Electrodeless Advanced Thruster (HEAT) project.[8)] Note that even though antenna s are outside of the plasma, we must consider the erosion problems[10)] in some cases.

Our propulsion system adopts a high-density helicon plasma generated by a helicon wave. As the radio frequency (RF) wave is applied from outside of a discharge cylinder, a discharge antenna does not contact with a plasma directly. For the higher thrust, the propulsion system need to accelerate a plasma and exhaust them into the space. The axial gradient of density is naturally exists in the generation part and a plasma is accelerated, and the magnetic gradient also exists in the

open-end of the parallel magnetic field by which the plasma is expected to be accelerated. In addition, our group has been studying some active acceleration methods to improve the thrust efficiency.[8] These methods produce an axial direction thrust F_z using the Lorentz force, i.e., the product of an induced azimuthal current j_θ and an external radial magnetic field strength B_r.[11,12] To demonstrate and optimize this system, it is also important to measure various plasma parameters. Laser Induced Fluorescence (LIF) method[13-16] can estimate velocity distribution functions of ions, atoms and molecules non-invasively with a high spatial resolution. It can also derive their temperatures, flow velocities and relative densities from the distribution functions. In a previous research, we have developed 2D LIF system to measure the plasma flow distributions.[17,18] This system had movable laser injection and fluorescence receiving optics for radial and axial scans.

To get spatial distributions of plasma flow conveniently, we have been developing a multi-channel LIF measurement device. This includes a fluorescence receiving array along the laser axis. With this aim, we have also adopted a Multi-Pixel Photon Counter (MPPC)[19] instead of a photo multiplier tube (PMT) conventionally used, because the former is simple, easy, and inexpensive, and it is also as sensitive as the latter.

In this research, we will show a development of LIF measurement system using a MPPC as an initial stage for a multi-channel system. Additionally, argon ion velocity in plasmas will be shown, depending on the magnetic field gradient in a downstream region by this LIF system. In this discharge, the observed plasma has a narrow, bright blue column, called "Blue Mode",[20,21] which has strong Ar ion emission light intensities for argon plasma. In addition, we have derived a thrust force from these results without active acceleration systems.

2. Principle of LIF measurement

2.1. LIF scheme

Our LIF system adopted a three-level scheme of ion particle,[14] which is shown in Fig. 1. Ar II (argon ion) is optically pumped by 668.43 nm (668.63 nm in vacuum) Laser light from $3d^4F_{7/2}$ metastable state to $4p^4D_{5/2}$ excited state. Then the ion in excited state decays to the $4s^4P_{3/2}$ state by emitting photons at 442.60 nm (442.73 nm in vacuum).

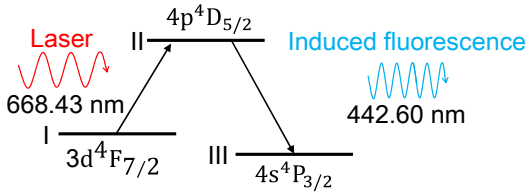

Fig. 1. LIF scheme of Ar II.

When a target particle have a velocity along a pumping laser axis, the excitation wave length is changed by a Doppler shift. Here, flow velocity and ion temperature of the target particles can be calculated in the following Eqs. (1) and (2). Additionally, relative density can be obtained from the area of IVDF.

$$\frac{c\Delta\nu}{\nu_0} = v \tag{1}$$

$$T_i = \left(\frac{\Delta\nu_{FWHM}}{2\sqrt{\ln 4}\nu_0}\right)^2 \frac{m_i c^2}{k} \tag{2}$$

3. Experimental Devices

3.1. Large Mirror Device (LMD)

Figure 2 shows the LIF measurement system on Large Mirror Device (LMD),[22] and Table 1 shows specifications and operating conditions of this device. The LMD has a tapered

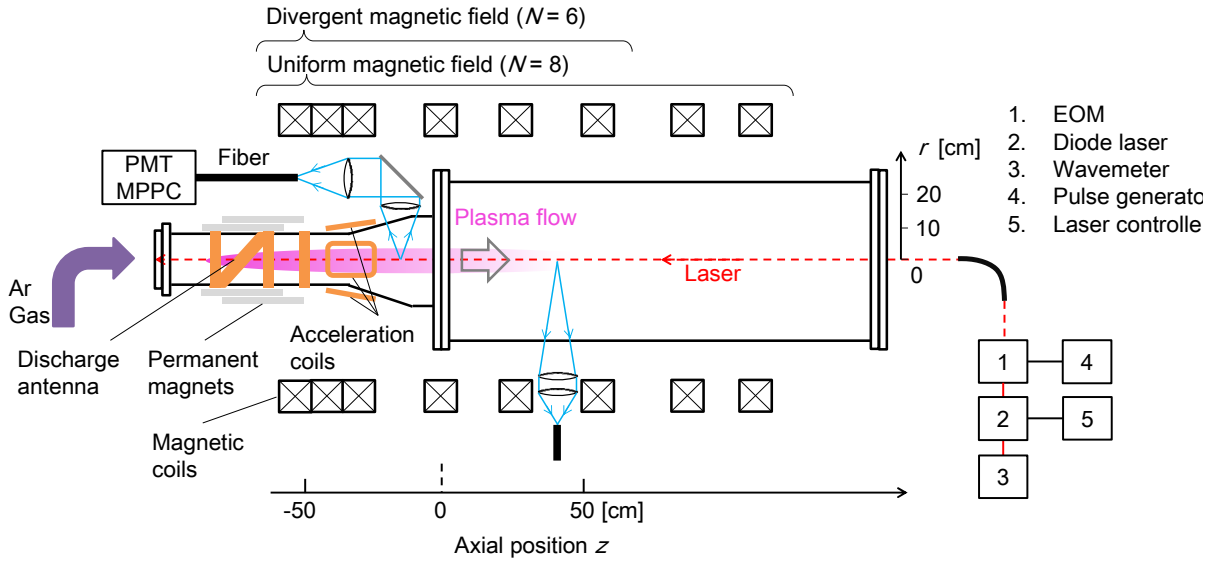

Fig. 2. LMD and LIF measurement system.

quartz tube connected to a main chamber. This tube has a discharge part, and its length L is 100 cm with its inner diameter i.d. of 10 ~ 17 cm. This tube length is long for accepting the acceleration system, e.g., rotating magnetic field (see accelerating coils in Fig. 2) and m = 0 coils[8]. Here, the tapered quarts shape is designed, considering the divergent of magnetic field configuration to reduce the wall loss of plasmas. The main SUS chamber (L = 170 cm and i.d. is 44.5 cm) is in a plasma diffusion region, and the left edge of this chamber is defined as the axial position of z = 0 cm. Here, the chamber has three square optical windows, and their center positions are z = 30, 60 and 90 cm. LMD has two turbo-molecular pumps, and their pumping speeds are 1,000 and 2,400 l/s, leading to a base pressure of ~ 10^{-4} Pa. When the gas is flowing with 90 sccm, the pressure is about 1 Pa at the head of the quartz tube and about 0.2 Pa at the end of the SUS chamber.

Table 1. Specifications and operating conditions of LMD.

Axial length	1,700 mm
Inner diameter of chamber	445 mm
Background pressure	~ 10^{-4} Pa
Propellant	Ar gas
RF input power	2.5 ~ 3.5kW
RF excitation frequency	7 MHz

A half-helical antenna is used to generate the plasma with a radio frequency (RF) input power R_{RF} of 2.5 ~ 3.5 kW at 7 MHz. The antenna has a matching network (split tank circuit), and the power transfer efficiency to the plasma is typically ~ 65 %. Two kinds of magnets are used for generating the various magnetic field configurations on LMD. The electromagnets (EMs) can produce external magnetic field B of 0 ~ 600 G flexibly and easily. Additionally, the permanent magnets (PMs) are also installed around the tapered quartz tube position where the strong B_r is obtained.[12] Note that the acceleration forces by $-\mu\nabla B$ and by $-\nabla p$ discussed in, e.g., 23), leads to ambipolar acceleration. This is related to the sum of plasma and magnetic pressures, and there can be considered as the acceleration forces. However, in this experiment, the divergence effect, i.e.,$\nabla B/B$, is not so high (see Fig. 3) to accelerate the plasma efficiently.

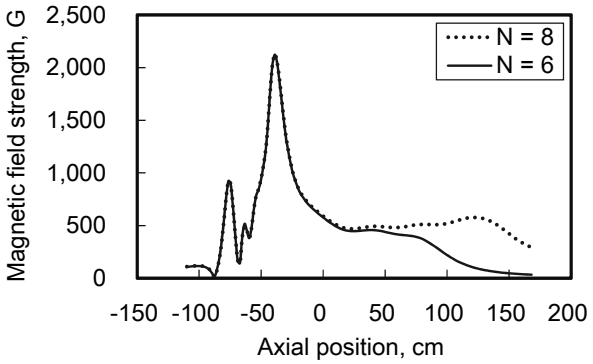

Fig. 3. Magnetic field strength for N = 8 and 6.

In order to see the acceleration effect in a downstream region by a ∇B force, LIF measurement has been carried out with a uniform field and a divergent magnetic field configurations. Figure 3 shows an axial profile of magnetic field strength, calculated by a FEMM[24] code. In the positive z region, the uniform magnetic field is generated by 8 magnets and the divergent one by 6 magnets. The blue mode plasma can be obtained in each magnetic field. Here, all the coil current in the experiments was 350A, with the coil voltage of 69 (53) V for N = 8 (6).

3.2. LIF measurement system

In a typical LIF measurement, a laser with a narrow bandwidth of frequency is necessary. The LIF system on LMD is shown in Fig. 2. The tunable diode laser used in these experiments is TA100 (TOPTICA Co.), which includes an oscillator and an amplifier. The laser wavelength width and its tuning range are 1 MHz and 663.5 ~ 669.3 nm, respectively.

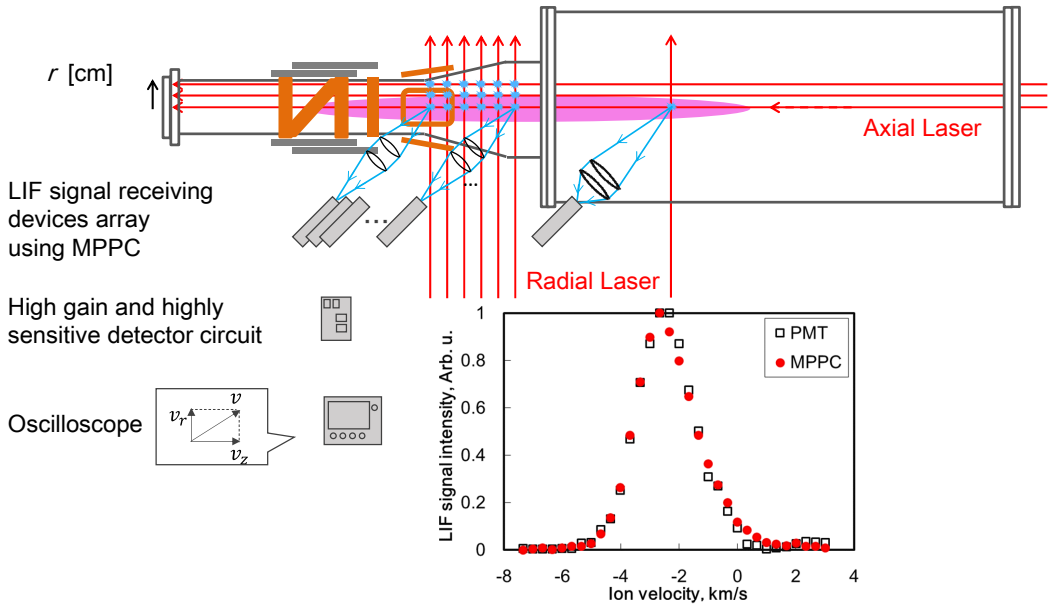

Fig. 4. A proposed plan of LIF multi-channel system.

The maximum output power is ~ 500 mW, and usually, it is operated at ~ 300 mW level. An injected real time laser frequency was monitored by the wavemeter WS7 (High Finesse / Angstrom Co.), whose wavelength accuracy is ± 0.1 GHz, corresponding to the velocity error of ± 66 m/s. In this experiment, an injected laser diameter via single-mode fiber is 5 mm. Signal receiving lenses of diameters are 100 mm with the focal lengths of 150 and 300 mm, and the diameter of an image at focal point with these lens is 3 mm. An absolute calibration of the wavelength, i.e. fundamental wavelength of non Doppler-shifted Ar II line of 443 nm was carried out by determining the middle point between Doppler shifts by the forward and backward laser injections using a reflecting mirror.

In order to separate a LIF signal from background noises including electric noise and background light of plasma, the laser light is electrically chopped by an Electro-Optic Modulator (EOM) LM0202 (LINOS PHOTONICS). The fluorescent emission is collected by a focus lens and optical fiber cables, and then it passes through a 4 nm bandwidth interference filter with a central wavelength at 443 nm to reach a high-gain sensitive optical device MPPC instead of PMT. The voltage signal passes through a high gain and highly sensitive detector circuit, and then goes to an oscilloscope. The Fast Fourier Transform (FFT) method is used to obtain the LIF signals modulated with a laser chopped frequency (455 kHz) by the EOM.

For our detailed investigation of plasma behavior at the same time, a plan of multi-channel measurement system, as shown in Fig. 4, is under development. In a laser injection system, a single-mode optical fiber is used because a flexible laser injection can measure a radial velocity distribution easily. In a signal receiving system, MPPC is adopted as a photodetector because MPPC is easy to use, inexpensive and as sensitive as a PMT. On the occasion of this modification, the above mentioned detector circuit developed (including effective lock-in amplifier circuit) amplifies the signal to derive Ion Velocity Distribution Functions (IVDF) with multi-channelization.

For realizing this concept, a single channel LIF signal receiving device with the MPPC and this laser measurement system using a single-mode optical fiber has been developed. The planned measuring region of 2D LIF system is z = 65 ~ -7 cm and r = 0 ~ 8 cm in a plasma source. Additionally, in the SUS chamber, positions of z = 30, 60 and 90 cm can be used for measurements. As shown in a graph inserted in Fig. 4, the measurement results using the previous system with the PMT and the new system with the MPPC show a good agreement. This was obtained under the condition that z = -20 cm, r = 0 cm, P_{RF} = 2.5 kW, and gas flow rate FR = 50 sccm.

4. Experimental Results

4.1. Ion Velocity Distribution Function (IVDF)

Figures 5 and 6 show the measured IVDF at z = 30 and 60 cm respectively with Gaussian distribution fitting curves. Here, Zeeman shifts for argon ions are ± 1.4 GHz/kG,[14,16] which shows a small effect on our measurements. A pulsed discharge plasma was operated with two kinds of magnetic field configurations, mentioned before. In this analysis, the signal intensity is normalized with the maximum value becomes one. In a pulsed plasma of 75 ms, we took the data in a period of 40 ~ 50 ms due to some instabilities in the initial phase of discharge. Each measurement was averaged over four successive plasma pulses, and from Eqs. (1) and (2), these plasma velocities and their temperatures were derived.

Here, argon ion velocity v_i was 0.17 km/s at z = 30 cm, and 0.067 km/s at z = 60 cm under the uniform magnetic field, which showed no acceleration effect. Under the divergent magnetic field, v_i was 0.095 km/s at z = 30 cm, 0.46 km/s at z = 60 cm, and 0.67 km/s at z = 90 cm. From this, acceleration effects of $-\mu\nabla B$ could be confirmed. Note that not only the effect of $-\mu\nabla B$ but also that of ∇p must be considered, as was mentioned. Argon ion temperature T_i was 0.16 eV at z = 30 cm and 60 cm under the uniform magnet field, while it was 0.15 eV at z = 30 cm, 0.11 eV at z = 60 cm and 0.072 eV at z = 90 cm under the divergent magnetic field. From this, T_i did not change under the uniform magnetic field, but it decreased with z under the divergent field.

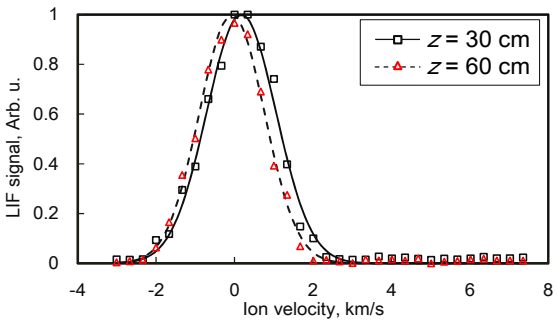

Fig. 5. Ion velocity distribution functions at z = 30 and 60 cm. with N = 8. P_{RF}: 3.0 kW, Gas flow rate: 90 sccm

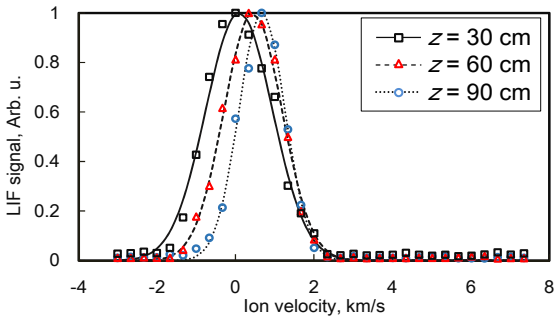

Fig. 6. IVDF at z = 30, 60 and 90 cm with N = 6. P_{RF}: 3.0 kW, Gas flow rate: 90 sccm.

Here, the measured velocity is small and it is approximately the same as the ion thermal velocity. We can list up four reasons as follows. First, the magnetic field of these experiments is not so much divergent and not optimized for the efficient acceleration. Second, the ions are decelerated by colliding with neutral particles and we need to estimate the behavior of neutral particles. Third, to verify the divergent

magnetic effect, the measurement of the radial velocity is needed. Fourth, the metastable argon velocity is not be the same as the real ion velocity.

4.2. Estimation of thrust

In order to calculate the thrust, we also need the radial electron density distribution, which was obtained by an electrostatic probe, as shown in Fig. 7. Because the blue mode plasmas were not obtained at P_{RF} = 3.0 kW, P_{RF} was increased to 3.5 kW.

The plasma thrust is derived as follows with this particle density.

$$F_i = \int m_i f(r,v) v_i^2 \, dvdr \quad (3)$$

$$\int f(r,v) \, dv = n_e(r) \quad (4)$$

Here, a constant value of v_i (by the present LIF method) was assumed in the same z position, and n_e was from this probe measurement. Under the divergent magnetic field, F_i was calculated to be 3.3 mN at z = 30 cm, 4.3 mN at z = 60 cm, and 3.1 mN at z = 90 cm. These values are not so much different from other small helicon plasma thrusters (0.5 ~ 5 mN/kW). [25-27] Of course, it is necessary to improve the thrust performance.

In addition, these values are not contradictory to our previous results using a target-type thrust stand.[28] However, we must consider the followings: 1) the effect of the thrust stand on the plasma performance, 2) the effect of neutral flow, and 3) the measurements from the center to the edge of plasma. We have a plan to measure the various parameters in the presence of the thrust stand.

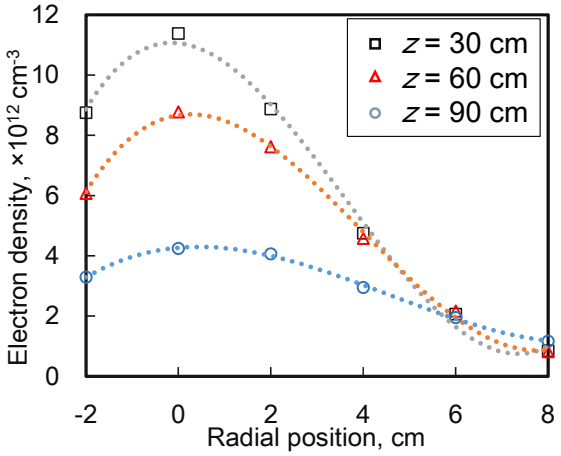

Fig. 7. Measured electron density by an electrostatic probe in blue mode plasmas. P_{RF} is 3.0 kW at z = 60 and 90 cm, and is 3.5 kW at z = 30 cm, with a gas flow rate of 90 sccm.

5. Conclusion

In order to estimate the electromagnetic acceleration method in an electrodeless propulsion system, we have been developing the multi-channel LIF system. A single channel LIF measurement system has been established, which includes a flexible laser injection system by optical fibers and a highly sensitive signal receiving device with a MPPC. We have carried out ion flow measurement by the LIF system using two magnetic field configurations. Plasma acceleration coming from $-\mu\nabla B$ effect was confirmed in the downstream region under the divergent field: ion flow velocity (ion temperature) was increased (decreased) with z. The plasma thrust was also estimated by the LIF system and the Langmuir probe, whose result was consistent with the direct thrust measurement. Though the estimated thrust in this paper is not sufficient for future application, the thrust itself is comparable to other present helicon plasma thrusters. Therefore, we must measure the plasma in our system in order to optimize this system: We are going to estimate various parameters using the multi-channel system developed with additional diagnostics of Langmuir probe, spectroscopy and a high-speed camera.

Acknowledgments

We appreciate useful discussions made by the HEAT project members. This study has been partially supported by Grant–in–Aid for Scientific Research (S: 21226019) from the Japan Society for the Promotion of Science.

References

1) Boswell, R. W.: Plasma Production Using A Standing Helicon Wave, *Phys. Lett.* **33A**, (1970), pp. 457-458.
2) Squire, J. P., Cassady, L. D., Chang Diaz, F. R., Carter, M. D., Glover, T. G., et al.: Superconducting 200 kW VASIMR Experiment and Integrated Testing, 31st Int. Electric Propul. Conf., IEPC-2009-209, 2009.
3) Squire, J. P., Olsen, C. S., Franklin. R., Diaz, C.,Cassedy, L. D., et al.: VASIMR® VX-200 Operation at 200kW and Plume Measurement: Future Plans and ISS EP Test Platform, 32nd Int. Electric Propul. Conf., IEPC-2011-154, 2011.
4) Charles, C.: A Review of Recent Laboratory Double Layer Experiments, *Plasma Sources Sci. Technol.* **16** (2007), pp. R1-R25.
5) Pottinger, S., Lappas, V., Charles. C., Boswell, R. W.: Performance characterization of a helicon double layer thruster using direct thrust measurements, *J. Phys. D: Appl. Phys.* **44** (2011), pp. 235201-1-235201-5.
6) Charles, C. and Boswell R. W.: Current-free Double-layer Formation in a High-density Helicon Discharge, *Appl. Phys. Lett.*,**82** (2003), pp. 1356-1358.
7) Batishchev, O. V.: Minihelicon Plasma Thruster, *IEEE Trans. Plasma Sci.*, **10** (2009), 1563.
8) Shinohara, S., Nishida, H., Tanikawa, T., Hada, T., Funaki, I. and Shamrai, K. P.: Development of Electrodeless Plasma Thrusters with High-Density Helicon Plasma Sources, *IEEE Trans. Plasma Sci.*, **42** (2014), pp. 1245-1254.
9) Kuninaka, H., Nishiyama, K., Funaki, I., Yamada, T, Shimizu, Y. and Kawaguchi, J.: Powered flight of electron cyclotron resonance ion engines on Hayabusa explorer, *J. Propul. Power,* **23** (2007), pp. 544-551.
10) Berisford, D. F., Benton, R. and Raja, L.: Power balance and wall erosion measurements in a helicon plasma, *Phys. of Plasmas*, **17** (2010), pp. 033503-1-033503-11.
11) Ishii, T., Ishii, H., Otsuka S., Teshigahara, N., Fujitsuka, H., Waseda, S., Kuwahara, D. and Shinohara, S.: Study on electrodeless electric propulsion in high-density helicon plasma with permanent magnets, *JPS Conf. Proc.*, **1** (2014), pp. 015047-1-015047-7.

12) Otsuka, S., Takizawa, K, Tanida, Y., Kuwahara, D. and Shinohara, S.: Study on plasma acceleration in completely electrodeless electric propulsion system, *Plasma Fusion Res.*, **10** (2015), pp. 3401026-1-3401026-4.
13) Severn, G. D., Edrich, D. A. and McWilliams, R.: Argon ion laser-induced fluorescence with diode lasers, *Rev. Sci. Instrum*, **69** (1998), pp. 10-15.
14) Boivin, R. W. and Scime, E. E.: Laser Induced Fluorescence in Ar and He Plasmas with Tunable Diode Laser, *Rev. Sci. Instrum*, **74** (2003), p 4352-4360.
15) Sun, X., Scime, E. E., Miah, M., Cohen, S. and Skiff, F.: Measurement of Asymmetric Optical Pumping of Ions Accelerating in Magnetic-Field Gradient, *Physical Review Lett.*, **93** (2004), pp. 235002-1-235002-4.
16) Keesee, A. M., Scime, E. E. and Boivin, R. F.: Laser-induced fluorescence measurements of three plasma species with a tunable diode laser, *Rev. Sci. Instrum*, **75** (2004), pp. 4091-4093.
17) Teshigahara, N., Shinohara, S., Yamagata, Y., Kuwahara, D. and Watanabe, M.: Development of 2D laser induced fluorescence (LIF) system in high-density helicon plasma, *Plasma Fusion Res.*, **9** (2014), pp. 3406055-1-3406055-4.
18) Kuwahara, D., Tanida, Y., Watanabe, M., Teshigahara, N., Yamagata, Y. and Shinohara, S.: Development of Ar I and Ar II Measuring System using Laser-Induced Fluorescence Methods in High-Density Helicon Plasma, *Plasma Fusion Res.*, **10** (2015), pp. 3401057-1-3401057-4.
19) Hamamatsu Photonics, MPPC® MPPC modules, (2014), p. 13.
20) Chen, F. F. and Boswell R. W.: Helicons - The past decade, *IEEE Trans. Plasma Sci.*, **25** (1997), pp. 1245–1257.
21) Chen, F. F.: Helicon discharges and sources, *Plasma Sources Sci. Technol*., **24** (2015), pp. 014001-1-014001-25. [Review Paper]
22) Shinohara, S., Takechi, S. and Kawai, Y.: Effects of axial magnetic field and Faraday shield on characteristics of RF produced plasma using spiral antenna, *J. Phys. Soc. Jpn.*, **35** (1996), pp. 4503-4508.
23) Fruchtman, A., Takahashi, K., Charles, C. and Boswell, R. W.: A magnetic nozzle calculation of the force on a plasma, *Phys. Plasmas*, **19**, (2012), 033507-1-033507-6.
24) FEMM, Finite Element Method Magnetics, Software Package, FEMM 4.2 64-bit Executable, Meeker, D., Walsome, MA, (2013).
25) Nakamura, T., Nishida, H., Shinohara, S., Funaki, I., Tanikawa, T. and Hada, T.: Preliminary Investigation of Electromagnetic Thrust Characteristics in Electrodeless Compact Helicon Plasma Thruster, *Trans. JSASS Aerospace Tech. Japan*, **12**, ists29 (2014), pp.Po_1-Po_6.
26) Ito, S., Nakamura, T., Nishida, H. and Shinohara, S.: Performance of RF Plasma Thruster for Various Magnetic Field Configurations by Permanent Magnets, 34th Int. Electric Propul. Conf., IEPC-2015-412, 2015.
27) Tonooka, S., Funaki, I., Matsuoka, T, Iwabuchi, S., Nakamura, T., Shinohara, S. and Nishida, H.: Thrust Characteristics of Helicon Plasma Thrusters, 33th Int. Electric Propul. Conf., IEPC-2015-253, 2013.
28) Kuwahara, D., Koyama, Y., Otsuka, S., Ishii, T., Ishii, H., Fujitsuka, H., Waseda, S. and Shinohara, S.: Development of direct thrust measurement system for the completely electrodeless helicon plasma thruster, *Plasma Fusion Res.*, **9** (2014), pp. 3406055-1-3406055-4.